Engineering Structures 211 (2020) 110499

Contents lists available at ScienceDirect

Engineering Structures

journal homepage: www.elsevier.com/locate/engstruct

# Evaluation of deformation-based seismic performance of RECC frames based on IDA method

Chang Wu[a,*], Zuanfeng Pan[b,*], Chenhua Jin[c], Shaoping Meng[a]

[a] School of Civil Engineering, Southeast University, Nanjing 211189, China
[b] College of Civil Engineering, Tongji University, Shanghai 200092, China
[c] School of Architectural Engineering, Jinling Institute of Technology, Nanjing 211169, China

ARTICLE INFO

*Keywords:*
Reinforced engineered cementitious composites (RECC)
Frames
Seismic performance
Performance-based Seismic Design (PBSD)
Incremental Dynamic Analysis (IDA)

ABSTRACT

Engineered Cementitious Composites (ECC) is a typical High Performance Fiber Reinforced Cement-based Composite (HPFRCC), which possesses the characteristics of ultra-high tensile ductility and energy dissipation capacity. One of the potential applications of ECC is to replace conventional concrete in the seismic resistant structures. However, to date, the investigation on seismic performance of ECC at the structural level is still limited. This paper aims at evaluating the seismic performance of RECC frame on the basis of Performance-based Seismic Design (PBSD) concept and discussing the feasibility and practicability of applying ECC in structures for improving the seismic performance. The non-linear behavior of ECC material was simulated especially considering the strain hardening behavior in tension. By using the Incremental Dynamic Analysis (IDA) method, three types of frames, consisting of a normal RC frame, a RECC frame and an RECC/RC composite frame, were analyzed to evaluate the structural dynamic behavior of the frames. Comparative studies on the deformation limit states at five levels of seismic performance for these three different types of frames validated that RECC frames have superior deformation capacity comparing to traditional RC frames under high intensity earthquake. Comparison results also indicated that rationally applying ECC in key region of the structures can not only improve the seismic performance and deformation capacity of structures but also control the construction cost.

## 1. Introduction

Engineered Cementitious Composites (ECC), generally consists of cement, mineral admixture, fine aggregates, water, admixtures which are used to enhance the strength and workability, less than 2% volume of short fibers, was first developed by Li et al. [1–3] based on the basic principle of micromechanics and fracture mechanics. Different from normal concrete with brittle tensile behavior and crack localization, ECC exhibits multiple fine cracks and strain-hardening behavior under tension. The opening of each crack is usually controlled to be less than 100 μm, and the ultimate tensile strain can reach over 3.0% [4–6]. A typical tensile stress-strain relationship of ECC is shown in Fig. 1. The ultra-high tensile ductility and energy dissipation capacity of ECC just remedy the shortcomings of concrete and thus attract the attentions of many researchers and designers around the world. ECC is being considered for replacing conventional concrete in structures in high-intensity earthquake regions [7–9]. Research efforts have focused on the seismic related behavior of ECC [10–18], however, the researches with respect to ECC are mostly limited to the material level and component level, while the investigation focusing on ECC at structural level is still at the preliminary stage. Gencturk et al. [19–20] established a constitutive model for ECC within Zeus-NL, and a two-story-two-span frame was simulated with the proposed model and tested under dynamic loading. Based on the analysis, seismic design parameters were derived using FEMA P695 methodology for two different special moment frames [21]. Yuan et al. [22] numerically modeled three frames with different matrixes under earthquake loading to verify the contribution of ECC to structural seismic resistance. The simulation results indicate that the application of ECC can reduce the maximum story drift ratio and the distributions of the dissipated energy are more uniform along the building height. Xu et al. [23] studied the seifsmic behavior of a precast ECC/RC composite frame and a precast RC frame with shaking table tests. Test results indicated that using ECC in precast frames can greatly reduce damage. Liang et al. [24] tested five beam-column–slab subassemblies with various column-to-beam flexural strength ratios, four of which used ECC at the joint and plastic hinge regions of the beam, column, and slab. The results indicated that the specimens contain ECC material had a greater tendency toward the “strong

* Corresponding authors.
*E-mail addresses:* changwu@seu.edu.cn (C. Wu), zfpan@tongji.edu.cn (Z. Pan).

https://doi.org/10.1016/j.engstruct.2020.110499
Received 3 July 2019; Received in revised form 7 March 2020; Accepted 7 March 2020
0141-0296/ © 2020 Elsevier Ltd. All rights reserved.

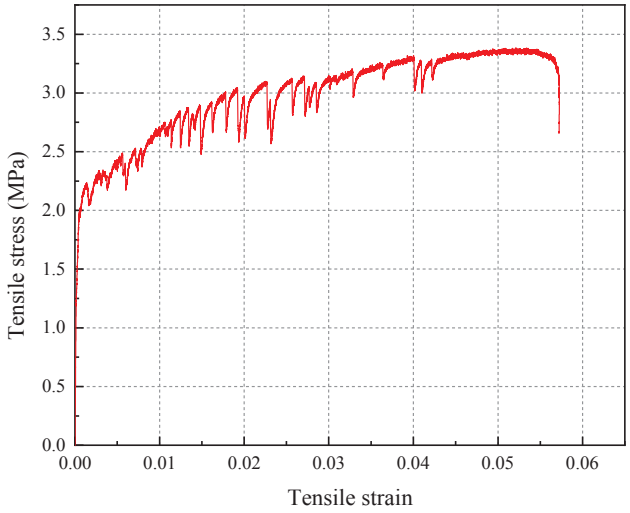


**Fig. 1.** Typical tensile stress-strain relationship of ECC.

column–weak beam" failure mechanism compared with the traditional RC specimens, and the use of ECC in the subassemblies enhanced their seismic performance with regard to energy dissipation, ductility, and integrity. Yu et al. [25] conducted shaking table tests on two one-quarter–scale two-story frame models: a RC frame and a frame of which the seismic vulnerable parts were made of plain UHDCC, with tensile strain capacity up to 10%, and the rest parts were normal RC. It is indicated that the UHDCC frame had a similar seismic resistance capacity to the reference RC frame and performed even better in vibration control. Compare to the research of ECC in material level and component level, the investigation of ECC at structural level is limited. The difficulty and expensiveness of full-scale structure tests is one of the reasons to restrict the investigation of ECC at structural level. Besides, models and programs for simulating the structural response of ECC structures under seismic loading are rather limited.

Incremental Dynamic Analysis (IDA) method, whose concept was first proposed in 1977 by Bertero [26], is one of the dynamical analysis methods for analyzing the response of structures under earthquake. In recent years, IDA method becomes more and more popular due to the significant development of computer technology. IDA method has become a powerful tool in the performance-based seismic design (PBSD) method to design and evaluate the seismic performance of structures. The IDA can capture the seismic demand and collapse resistant capacity of structures under earthquakes with different levels of intensity, and therefore a comprehensive evaluation of the seismic performance of a structure can be fulfilled based on the whole analyzed structural responses including the elastic stage, elastic-plastic stage and final collapse. IDA method is now widely used in the nonlinear analysis of structures under earthquake [27–31], and FEMA-356 [32] has adopted IDA method as an analysis approach to evaluate the seismic performance and collapse resistant capacity of structures.

This paper aims at evaluating the seismic performance of RECC frame on the basis of PBSD concept using IDA method. The cyclic constitutive model of ECC was implemented to OpenSEES, and three types of frames, consisting of a normal RC frame, a RECC frame and an ECC/RC composite frame, are analyzed with IDA method to validate the superiority of ECC structures in terms of seismic performance under various performance levels. By comparing and analyzing the multi-record IDA curves of each frame, the deformation limit state of the frames under five levels of seismic performance are discussed and suggested. Moreover, the feasibility and practicability of applying ECC in structures for improving seismic resistance and controlling the construction cost are preliminarily discussed.

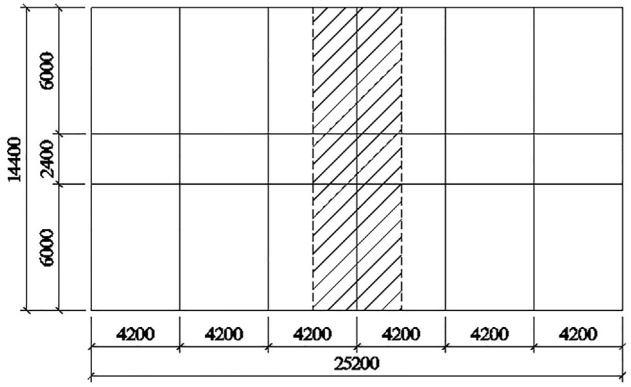


**Fig. 2.** Diagram of plane layout of analyzed frame structure.

## 2. Computational modeling

### 2.1. Information of the analyzed frames

Three frames including a normal RC frame, an ECC frame and an ECC/RC composite frame were analyzed with IDA method. The plan view of the building model is given in Fig. 2. Since the layout of the structure is regular in both plan and vertical views, a single 2D frame is isolated as the analysis object, as shown in Fig. 3. The bottom story height is 3.9 m, while other stories are 3.3 m high. The reference frame was designed based on Chinese code for design of concrete structures (GB50010-2010)[33]. The cross section of all beams was unified to 300 mm (width) × 500 mm (height), and all columns have 500 mm × 500 mm cross-sectional dimensions. The beams contain three 20 mm diameters longitudinal reinforcing bars in both top and bottom of the sections and 10 mm-diameter rebars with spacing of 100 mm for stirrups; while the columns lay out eight longitudinal reinforcing bars with diameter of 20 mm and 10 mm-diameter rebars with spacing of 75 mm for stirrups (see Fig. 3 for details). All the frames have the same geometry and reinforcement layout. For comparison, the compressive strengths of both concrete and ECC were assumed to be 35 MPa. And the yield strengths of longitudinal and transverse reinforcing bars were assumed to be 400 MPa and 335 MPa, respectively.

### 2.2. Finite element modeling of the frames

In this study, the open source FEA software OpenSEES is used to apply incremental dynamic analysis. A single RC frame, an ECC frame

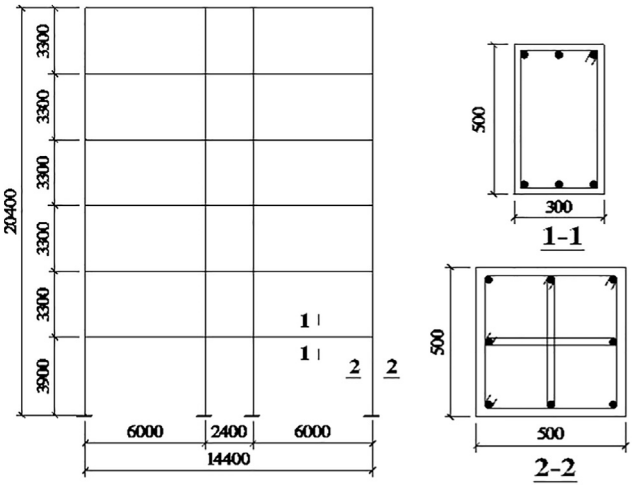


**Fig. 3.** Elevation of the frame and reinforcement details for beams and columns.

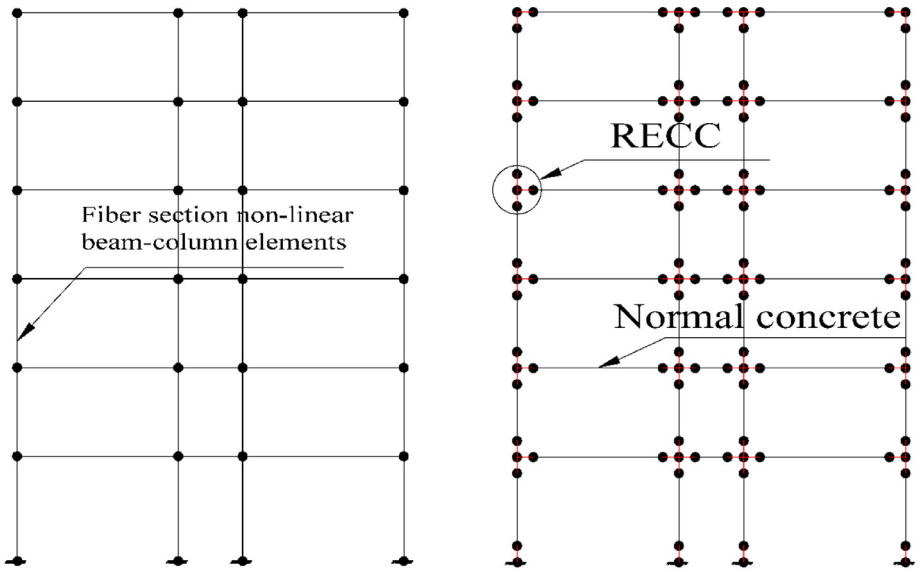


**Fig. 4.** FEM models of the frames.

and an ECC/RC composite frame were extracted from the reference building respectively and modeled with 2D elements for simplicity. Traditional concrete and ECC were utilized in the beams and columns for RC frame and ECC frame respectively (see Fig. 4(a)). The RECC/RC frame was applied with ECC material in joint and plastic hinge area, including joint core area and plastic hinge area, defined as extended length in beams and columns that equal to the height of the corresponding cross-section, and the area in the bottom end of columns up to length one time as the height of column cross-section, while other part of the frame were made by traditional concrete (see Fig. 4(b)).

The beams and columns in the frames were modeled with fiber section nonlinear beam-column element included in OpenSEES. Fiber section based element allows users to divide the section into several fiber elements and assign different material properties. In addition, reinforcing bars in concrete can be modeled by setting additional integral points in the cross-section. In this study, the section of each reinforced concrete member was modeled with confined concrete fibers, unconfined concrete fibers and steel bar fibers, as shown in Fig. 5. The confinement factor in concrete core area can be determined with the relevant formula in modified Kent-Park model, and in this study, the confinement factor was set to be 1.1 for simplicity. For RECC members, ECC fibers in cross-section do not differentiate between confined and unconfined area, because the fiber bridging effect due to the randomly distributed fibers in ECC can provide strong confinement and consequently the confinement effect by stirrups becomes no more effective.

Modal analyses were first applied to check the finite element models. The analysis results show that the RC frame (named as F0) has a basic period of 0.72 s; while the basic period of ECC frame (named as F1) is 0.96 s, which is larger than the former. This is mainly resulted by the relatively lower modulus of elasticity of ECC material compared to traditional concrete. The basic period of ECC/RC composite frame (named as F2) was calculated to be 0.85 s, which falls in between the basic periods of RC frame and ECC frame. The information of analyzed frames are shown in Table 1.

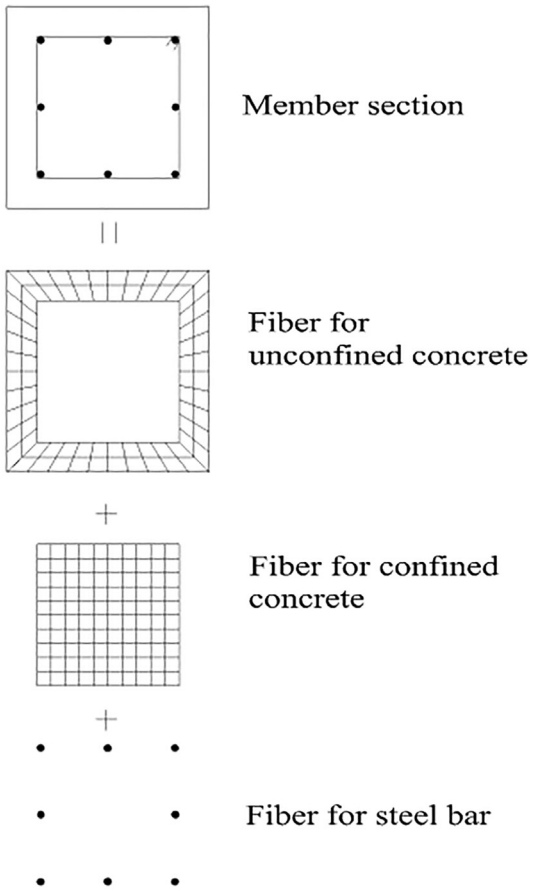


**Fig. 5.** Fiber section model.

### 2.3. Cyclic uniaxial constitutive model for ECC

The cyclic uniaxial constitutive model for ECC material in compression and tension applied in this study are given in Fig. 6 [34,35]. The tensile stress-strain relationship was characterized by a trilinear model, in which three distinct branches consisting of linear elastic stage, pseudo tensile strain-hardening stage and softening stage were expressed. The compressive stress-strain relationship was developed using the form of parabolic curve for the ascending branch and the bilinear form for the descending branch. The characteristics of

**Table 1**
Basic information of the analyzed frames.

| Frame number | Material | Regions applied with ECC | Basic period (s) |
|---|---|---|---|
| F0 | RC | None | 0.72 |
| F1 | ECC | All members | 0.96 |
| F2 | RC and ECC | Joint and plastic hinge areas | 0.85 |

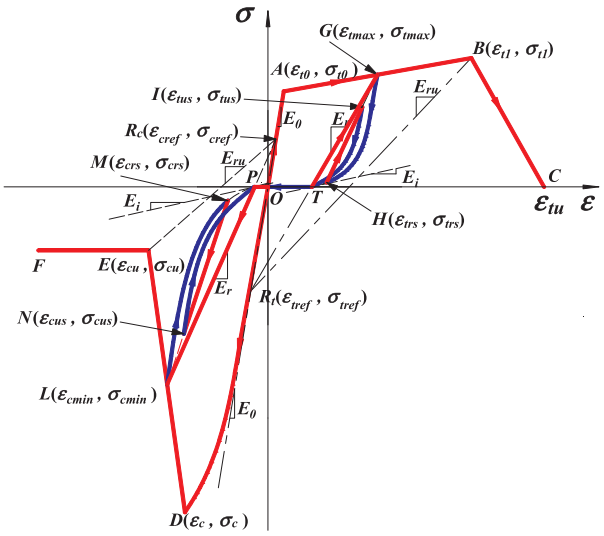


**Fig. 6.** Stress-strain curve of ECC under cyclic loading.

unloading and reloading process were determined by setting a reference point. The accuracy of the constitutive model was verified through the unloading and reloading experiment of SHCC samples. More details for the cyclic uniaxial constitutive model can be found in Wu, et al. [34]. In this analysis, the tensile strength of ECC and concrete was both set to be 0.1fc, where fc is the compressive strength. The tensile strain capacity of ECC was valuated to be 3%, while the compressive strain corresponding to the peak compressive stress was set to be 0.005 rather than 0.002 for normal concrete.

### 2.4. Selection of ground motion records

The determination of one single IDA curve depends on a series of time-history analyses by inputting one ground motion with multiple amplitudes. To avoid the error due to the randomness of one single ground motion record (GMR), multiple GMRs are applied in IDA, and results obtained from IDA should be analyzed statistically. Although the use of multiple GMRs can take into account the difference of inputting various GMRs in some extent, the selection of GMR will influence the analytical results directly, since the ground motion is generally uncertain due to the effects of multiple factors including the seismogenic mechanism, propagation medium, site condition, etc. And thus, reasonable selection of GMRs becomes important in IDA.

In this study, fourteen GMRs under strong earthquake were selected based on ATC-63 [36], in which a scientific research-oriented method for selecting the GMRs was suggested. These GMRs all comes from earthquakes with magnitude 6.5 or above, and their seismic fault distance are greater than 10 km for diminishing the influence of near-field effect. The average shear-wave velocities in the top 30 m ($V_{s30}$) of the selected earthquake waves range from 200 m/s to 500 m/s. Meanwhile two artificial ground motions which statistically coincide with the design response spectrum in GB50011-2010 [37]. Therefore, total 16 earthquake waves were selected as the input ground motion in IDA. The information of the selected earthquake waves are listed in Table 2, while the pseudo-acceleration response spectrums for the selected earthquake waves are shown in Fig. 7.

**Table 2**
The GMRs applied in the IDA.

| # | GMR name | Date | PGA/g | PGV/cm/s | PGD/cm | $V_{s30}$/m/s | $\Delta_e$/km |
|---|---|---|---|---|---|---|---|
| 1 | Friuli, Italy | 1976 | 0.31 | 30.78 | 5.08 | 424.8 | 14.97 |
| 2 | Northridge | 1994 | 0.88 | 41. 69 | 14.65 | 336.2 | 17.28 |
| 3 | Duzce, Turkey | 1999 | 0.82 | 62.07 | 13.55 | 326 | 12.02 |
| 4 | Chi-Chi | 1999 | 0.38 | 62.02 | 51.73 | 446.6 | 45.15 |
| 5 | Chi-Chi | 1999 | 0.26 | 52.1 | 48.07 | 401.3 | 19.02 |
| 6 | Kobe | 1995 | 0.34 | 27.64 | 9.6 | 312 | 22.5 |
| 7 | Kobe | 1995 | 0.24 | 37.84 | 8.54 | 256 | 19.14 |
| 8 | Landers | 1992 | 0.42 | 42.3 | 13.85 | 271.4 | 19.74 |
| 9 | Imperial Valley | 1979 | 0.35 | 32.99 | 18.88 | 274.5 | 22.03 |
| 10 | Superst.Hills | 1987 | 0.21 | 34.51 | 21 | 207.5 | 23.85 |
| 11 | Loma Prieta | 1989 | 0.37 | 44.63 | 19.29 | 349.9 | 12.23 |
| 12 | Loma Prieta | 1989 | 0.37 | 62.3 | 30.3 | 370.8 | 27.67 |
| 13 | Northridge | 1994 | 0.48 | 45.37 | 12.5 | 308.6 | 11.39 |
| 14 | Northridge | 1994 | 0.57 | 52.54 | 8.82 | 450.3 | 20.1 |
| 15 | Artificial wave 1 | – | 0.44 | – | – | – | – |
| 16 | Artificial wave 2 | – | 0.42 | – | – | – | – |

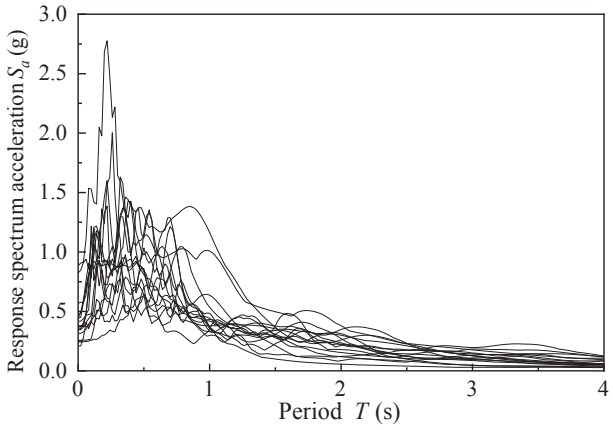


**Fig. 7.** The pseudo-acceleration response spectrums for the earthquake waves.

### 2.5. IDA procedure with OpenSEES

For applying dynamic analysis with OpenSEES, integral method, iterative algorithm and convergence criterion need to be set in advance. Newmark-$\beta$ method was applied as the integral method in IDA. To ensure the convergence, multiple iterative algorithms were preset, such as Newton-Raphson method, Modified Newton-Raphson algorithm, Krylov-Newton algorithm, Newton with Line Search Algorithm, Broyden Algorithm, BFGS Algorithm, etc. Once the analysis in a step point can not converge with one algorithm, another algorithm was tried until all the preset algorithms were applied. The analysis at one step ended when convergence can not be obtained after all the algorithms were tried. The energy increment test method is applied as the convergence criterion. In addition, masses of the members were concentrated in the beam-column joints for simplicity, and Rayleigh damping was applied to form damping matrix. Prior to each time-history analysis step in IDA, static analysis considering vertical loading was applied and the resulted structural response was considered as the initial state of the dynamic analysis. *P-Δ* effect was also considered in the analysis.

After setting the analysis parameters, a series of IDA can be conducted with the following procedure:

Build the FEM model of the frame and set proper cyclic constitutive model of the applied materials.
Determine a scale factor with “hunt and fill” algorithm [27] and compute the IM, and Input a selected GMR scaled with the scale factor and run the time-history analysis.
Output the DM related to the structural response with computed IM.

Repeat ②~③ until a single-recorded IDA is completed, and plot the recorded points in the coordinate system, in which DM is considered as horizontal axis while IM is considered as vertical axis.

By connecting the points in ascending order of IM, a single-record IDA curve is then obtained. Cubic spline interpolation is applied to smooth the curve, if the data points are rather limited.

Change a GMR and Repeat ②–⑤, then the multi-recorded IDA curves can be obtained.

Statistically analyze the multi-record IDA curves and calculate the quantile IDA curves of 16%, 50% and 84%.

### 2.6. Determination of performance levels and limit states

Referring to the classification of performance levels in Classification of earthquake damage to buildings and special structures (GB/T 24335-2009) [38], Code for seismic design of buildings (GB50011-2010)[37] and FEMA356 [32], the seismic performance of RECC frame is classified to five levels, which corresponds to the “almost intact”, “insignificantly damaged”, “moderately damaged”, “seriously damaged”, and “nearly collapsed”, respectively. The definition of the first four levels basically coincide with GB/T 24335-2009 and GB50011-2010, while the performance level (PL) V coincide with the level of Collapse Prevention (CP) defined in FEMA356.

The determination of the limit states corresponding to each structural performance levels are based on the resulted IDA curve. And the DM-based approach is applied in this study, and the classification of structural performance level and limit state points based on IDA curve is shown in Fig. 8. The definition rule for the limit states of deformation at different performance levels also refers to GB/T 24335-2009, GB50011-2010 and FEMA356, listed in Table 3, in which, $[\Delta\mu_e]$ and $[\Delta\mu_p]$ are defined as limits of elastic deformation and plastic deformation, respectively. In this study, the relevant deformation (or DM) is the maximum interstory drift angle.

## 3. Analytical results

### 3.1. IDA curves

The maximum interstory drift angle, $\theta_{max}$, was selected as DM; while PGA and $S_a(T_1, 5\%)$ were considered as IM respectively. In this study, PGA was adopted as IM to compare the seismic intensities for different frames reaching the same value of DM; and the $\theta_{max}$-$S_a(T_1, 5\%)$ IDA curves were used to determine the different performance levels for the frame structures. The IDA curves are shown in Figs. 10–12. All the IDA curves were treated with spline interpolation to let the curves smoother. And the maximum scale of $\theta_{max}$ is set to be 0.15, at which all the IDA curves were divergent, i.e., the slope of each curve became horizontal.

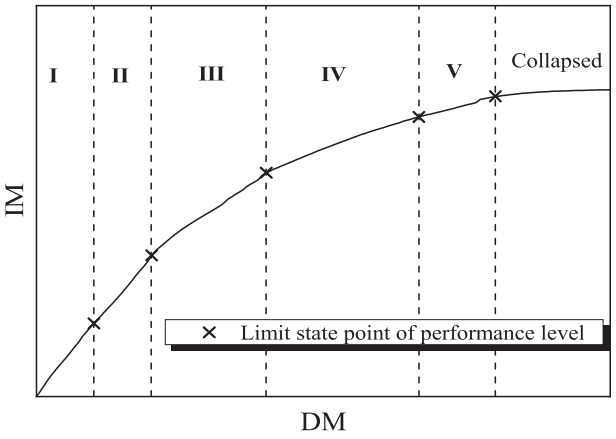


**Fig. 8.** Classification of Performance levels and limit state points.

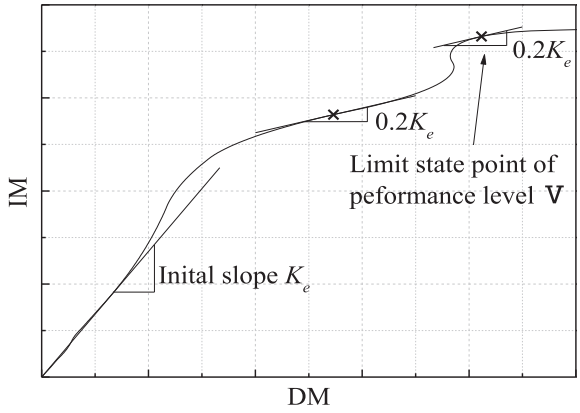


**Fig. 9.** Determination of the limit state point at PL V.

The figures show that although the shapes of the IDA curves are different, each IDA curve can be differentiated to initial elastic phase and gradually dynamic unstable phase with the incensement of PGA or $S_a(T_1, 5\%)$. When the three frames nearly collapse, i.e. the tangential slope of an IDA curve is degraded to the 20% of the initial tangential slope, all the maximum interstory drift angles for the frames are greater than 2%, which shows remarkable deformation capacity for the three frames subjected to strong earthquake. The detailed evaluation and comparison of deformation capacity will be discussed in the following sections. The figures also show that the variation of the IDA curves is higher for the curves with IM of PGA than that of $S_a(T_1, 5\%)$, especially in the early stage.

Since different earthquake recorders produce different IDA curves in a set of multi-record IDA Curves, statistics method should be used to make the IDA curves reasonably reflect the structural response. There are two main methods for estimating statistics of a sample of 2D random lines, which are parametric method and non-parametric method [27,28]. In this study, the non-parametric method is applied to summarize each set of IDA curves by defining 16%, 50% and 84% quantile IDA curves. For better comparing the seismic performance, $\theta_{max}$-PGA based IDA curves of the three frames at each quantile were summarized in Fig. 13(a)–(c), respectively. It can be seen from the figures that at the very beginning when PGA is at a low level, all the frames remain elastic condition and the IDA curves are close to each other. At the elastic stage, the probability IDA curves of RC frame are slightly higher than other two frames’ due to the higher modulus of elasticity of concrete. With the increase of $\theta_{max}$, plastic deformations are found in frames, and consequently the probability IDA curves of the three frames begin to differentiate. The slope of the IDA curve of frame F0 decreased rapidly after a certain value of $\theta_{max}$ is reached; whereas the slopes of the IDA curves of frames F1 and F2 just decrease gradually, and therefore, their IDA curves grow higher than the curve of RC frame. When the curves gradually turn horizontal, it can be observed that the IDA curves of ECC/RC composite frames lie a little lower than ECC frame’s IDA curve. The description above qualitatively indicates that when the frames close to collapse, the PGA satisfies the relation: $PGA_{F0} < PGA_{F2} < PGA_{F1}$, i.e. ECC frame and ECC/RC frame can undergo more intensive earthquake than normal RC frame.

### 3.2. Distribution of interstory drift angle

In this section, the distributions of interstory drift angle along with increasing IM for the frames were analyzed. For saving the length of the article, three representative responses corresponding to No. 1, No. 2 and No. 5 earthquake recorders were considered in detail. Figs. 14–16 show the development of interstory drift angle envelopes relating to different IMs (PGAs) in the three earthquake recorders.

**Table 3**
Classification and definition rules of performance levels and limit state points.

| Performance level | Definition | Limit state of deformation | IDA-based rule for determining the elastic and plastic deformations |
|---|---|---|---|
| I | almost intact | $[\Delta\mu_e]$ | The maximum deformation in the linear phase in IDA curve. |
| II | insignificantly damaged | $2[\Delta\mu_e]$ | – |
| III | moderately damaged | $([\Delta\mu_e] + [\Delta\mu_p])/2$ | – |
| IV | seriously damaged | $0.9[\Delta\mu_p]$ | – |
| V | nearly collapsed | $[\Delta\mu_p]$ | The deformation at which the tangential slope in the IDA curve is 20% of the initial slope. When multiple points satisfy the requirement, the point that is closest to the horizontal phase is selected (See Fig. 9). |

From Figs. 14–16, when the PGA kept in a low level for all the three earthquake recorders, the distributions of interstory drift angle were almost uniform, i.e., no story yielded and the maximum displacement of each story were nearly the same. With the increasing PGA, one story of each frame started to yield successively. However, for different earthquake recorders, the initial yielding of the frames usually occurs in different stories; moreover, even with the same earthquake recorder, different frames may not yield initially in the same story. For instance, the fifth story of each frame first yielded under the No.1 ground motion recorder; however, for No.2 earthquake recorder, ECC frame first yielded in the bottom story, while others yielded in the second and third stories. It can be also seen that the location of the maximum $\theta_{max}$ would change with the increasing PGA. Although the first yielded story located in the fifth story of the frames under No.1 earthquake recorder, the maximum $\theta_{max}$ then changed to the first story when the structures failed. The change of maximum $\theta_{max}$ story leads to the "hardening behavior" and twist of the corresponding IDA curve. For No.2 earthquake recorder, the maximum interstory drift angle at failure located as the same as the first yield story for RC frame and ECC frame, but in different stories for ECC/RC composite frame. In this case, the maximum $\theta_{max}$ remained in the same storey after yielding for RC frame and ECC frame, and the corresponding IDA curves showed "softening behavior"; while the IDA curve of ECC/RC composite frame exhibited hardening and twist behavior due to the alteration of the location of the maximum $\theta_{max}$. For No.5 earthquake recorder, the maximum $\theta_{max}$ varied between the first to the third story with the increase of PGA for all the three frames, and finally the frames failed when the maximum $\theta_{max}$ located in the second story for RC frame and ECC frame and the first in the first story for ECC/RC composite frame, respectively. The frequent change of maximum $\theta_{max}$ story resulted in the weaving behavior of related IDA curves for each frame.

The interstory drift angle distribution of the frames under all other earthquake recorders can be included in the representative responses mentioned above. And the analysis shows that the $\theta_{max}$ usually located in the second story and below, especially when the structures close to fail. Although the bottom story undertook the maximum shear force, the maximum $\theta_{max}$ sometimes occurred in second or third stories at failure due to the higher confinement and storey height. And by comparison, RECC frame shows the highest interstory drift capacity, followed by ECC/RC composite frame, both of which performed improved deformation capacity compared with normal RC frame.

### 3.3. The sequence and distribution of plastic hinges

The degree of plastic deformation of structures can be reflected by the distribution of plastic hinges. In this study, the criterion of appearance of plastic hinge is determined by the level of strain in the sectional fiber representing for steel rebar at member ends. If the yield strain of steel reinforcing bar is researched, the corresponding member end is considered as a plastic hinge. Also, due to the limitation of the article length, taking the responses under No.1 earthquake recorder as an example, the distribution of plastic hinges at beam and column ends for each frame was analyzed. Figs. 17–19 show the distribution of plastic hinges at three different levels of PGA for the three frames.

By defining the ratio of plastic hinge, $r_p$, as the number of plastic hinges to the total number of member ends, it can be seen from the figures that when PGA = 0.36 g, RC frame contains the most number of plastic hinge, with the $r_p$ of 11% (14% of ratio of plastic hinge in beam ends ($r_{pb}$) and 8% of ratio of plastic hinge in column ends ($r_{pc}$), respectively). The plastic hinges of RC frame mainly distributed at column bottom at first story, column ends at the fourth and fifth stories, and beam ends at the third and fourth floors under this PGA level. While the plastic hinges of ECC frame mainly distributed at bottom of the column and beam ends in the first story, and the plastic hinges of ECC/RC composite frame mainly distributed at the fourth and fifth stories. When PGA = 0.52 g, the fourth and fifth stories contained the most plastic hinges for each frame, and the plastic hinges spread to other stories with the increasing PGA due to the redistribution of internal forces in the structures. When the PGA of each frame reached the related critical value, at which the structure is about to collapse, most of the member ends formed plastic hinges. For RC frame, the ratio of plastic hinge in beam ends $r_{pb}$ = 89%, the ratio of plastic hinge in column ends $r_{pb}$ = 96% and the total ratio of plastic hinge $r_p$ = 93% when PGA = 1.82 g; for ECC frame, $r_{pb}$ = 89%, $r_{pb}$ = 83% and

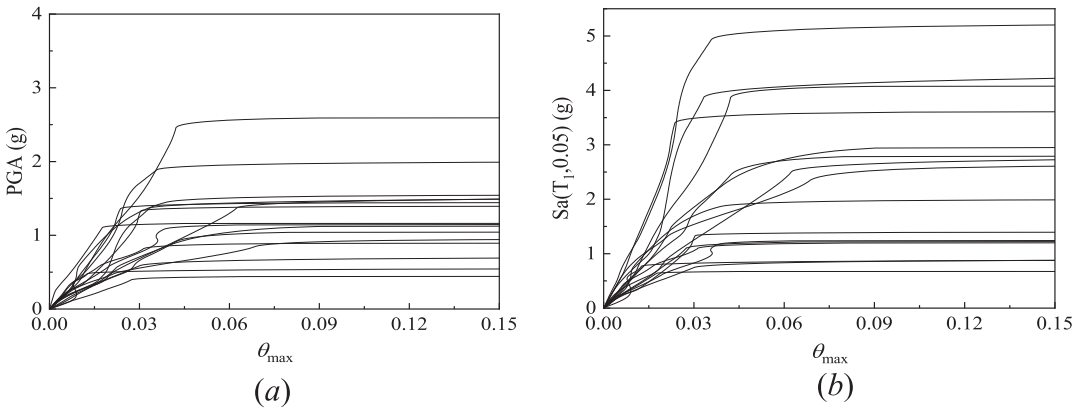


**Fig. 10.** Multi-recorded IDA curves of RC frame.

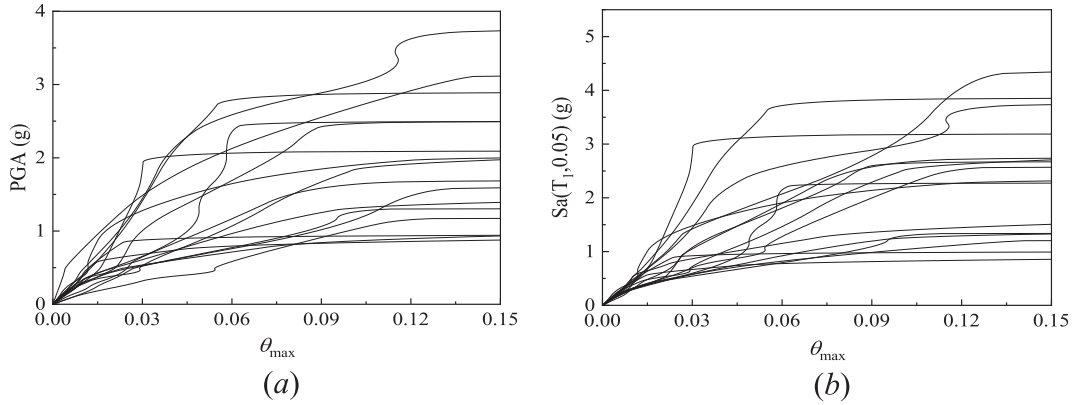


**Fig. 11.** Multi-recorded IDA curves of ECC frame.

$r_p$ = 86% when PGA = 3.12 g; for ECC/RC composite frame, $r_{pb}$ = 94%, $r_{pb}$ = 96% and $r_p$ = 95% when PGA = 2.47 g.

The sequence and distribution of plastic hinges of the three frames show that although the fourth and fifth stories formed most plastic hinges at early stage, the largest interstory drift occurred in the bottom story when the structure nearly collapsed, since the seismic load along the stories redistributed with the change of structural stiffness in stories. This indicates that the rotation of a plastic hinge is not only dependent on the sequence and location, but also effected by the change of structural stiffness. It can be also observed that under No.1 earthquake recorder, both beam and column ends formed plastic hinges, and the plastic hinges almost distributed in all the beam and column ends when under a high level of PGA. Fig. 20 shows the ratio of plastic hinge vs. PGA curves of three frames. We can see that when PGA < 1 g, the ratios of plastic hinge for the three frames were very close; and when PGA exceeded 1 g, the ratio of plastic hinge of ECC frame increased more slowly than other two frames and the final ratio of plastic hinge was also lower.

The ratio and distribution of plastic hinges exhibit obvious difference under different earthquake waves, which reflects different mechanism of collapse of the structure. If the ratio of plastic hinge is large, the structure may collapse globally as a result of dynamic instability of the entire structure; while if the ratio of plastic hinge is small, the plastic hinges may be localized in certain stories, in which excessive rotation of the plastic hinges may result in local dynamic instability, and consequently lead to the local collapse or progressive collapse of the structure.

Comparing the mean plastic hinges at the PL V point, as shown in Fig. 21(a), RC frame has the largest ratio, 74%; while the mean ratios for ECC frame and ECC/RC composite frame are very close and both lower than the ratio of RC frame, and the ratios are 68% and 67%, respectively. This indicates that more members may be damaged under moderate or strong earthquakes for RC frames, which increase the difficulties in repairing and retrofitting; while fewer members may be damaged in ECC frame or ECC/RC composite frame attributed to the larger rotation capacity of the plastic hinges, which is beneficial to the repairing and retrofitting work after earthquake.

Defining $\theta_{max0}$ as the maximum interstory drift angle at which plastic hinge initially arisen, $\theta_{max0}$ of RC frame is 0.73%, which is the lowest, RECC frame has the largest $\theta_{max0}$, which is 0.94%, and $\theta_{max0}$ of RECC/RC composite frame is 0.83%, as shown in Fig. 21(b). It should be noted that the value of $\theta_{max0}$ mentioned above may not be the exact value, since the data points are very limited in IDA, i.e., initial plastic hinge may arise prior to the analysis step point of the IDA in reality. Nevertheless, conclusions can be drawn that larger deformation are permitted for frames constructed with ECC or ECC/RC composite than traditional RC frames, under small or moderate earthquake.

### 3.4. Limit state of maximum interstory drift angle

According to the rules introduced in previous section, the five performance level critical points for the three types of frames were determined from the corresponding 16%, 50% and 84% quantile $\theta_{max}$-$S_a$ ($T_1$, 5%) IDA curves, as shown in Fig. 22. By comparing the IDA curves at 16%, 50% and 84% quantile, for all the frames, the maximum interstory drift angles at the PL I point in 16%, 50% and 84% quantile IDA curves are basically coincided, because only elastic deformation will be generated in the stage of PL I. But at the PL V point, the corresponding maximum interstory drift angles increase with the rise of quantile. For safety reason, the corresponding $\theta_{max}$ on 16% quantile IDA curve are chosen as the limit angle at the PL V point for the three frames.

Table 4 lists the analytical values of $\theta_{max}$ at each performance level

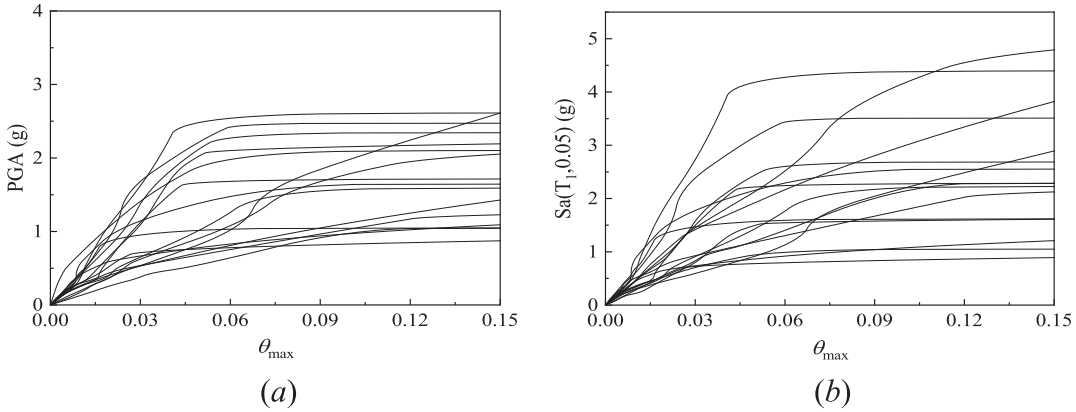


**Fig. 12.** Multi-recorded IDA curves of ECC/RC composite frame.

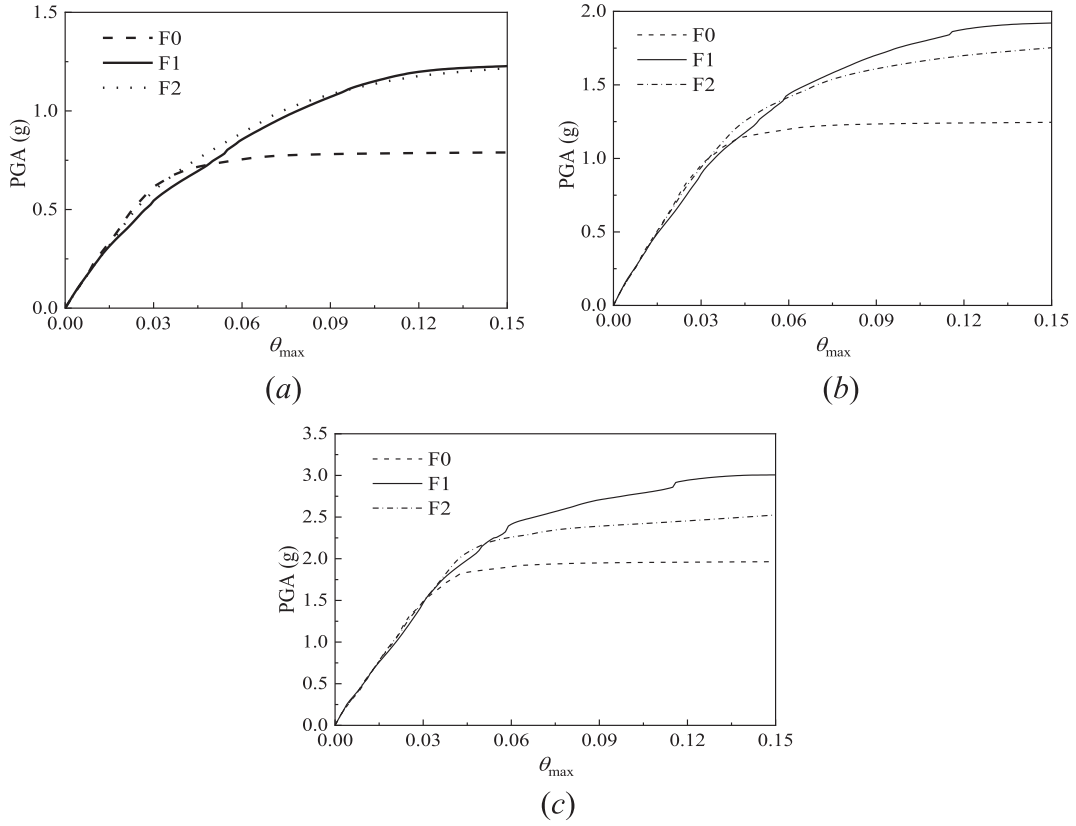


**Fig. 13.** Comparison of IDA curves of the three types of frames at (a) 16% quantile; (b) 50% quantile; (c) 84% quantile.

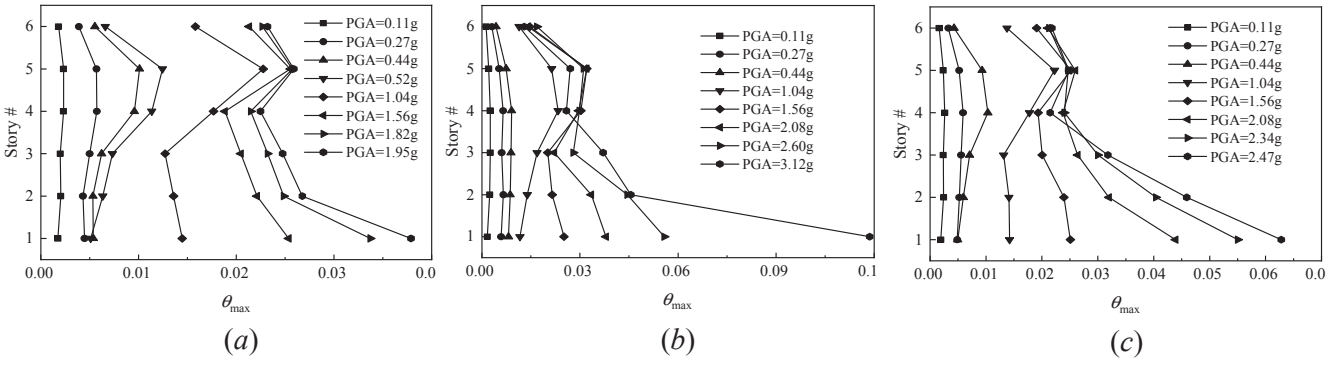


**Fig. 14.** The envelope diagram of $\theta_{max}$ in all stories under #1 earthquake wave for the analyzed frames (a) F0; (b) F1; (c) F2.

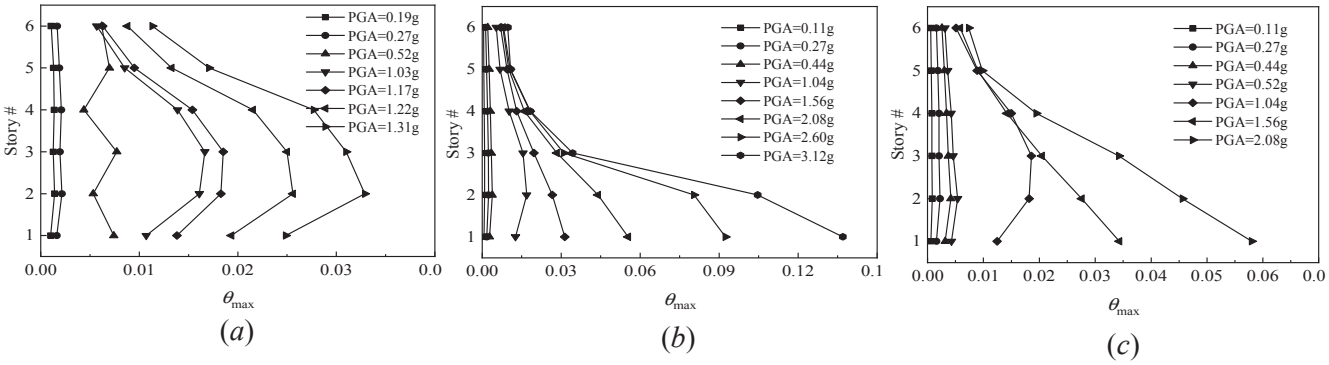


**Fig. 15.** The envelope diagram of $\theta_{max}$ in all stories under #2 earthquake wave for the analyzed frames (a) F0; (b) F1; (c) F2.

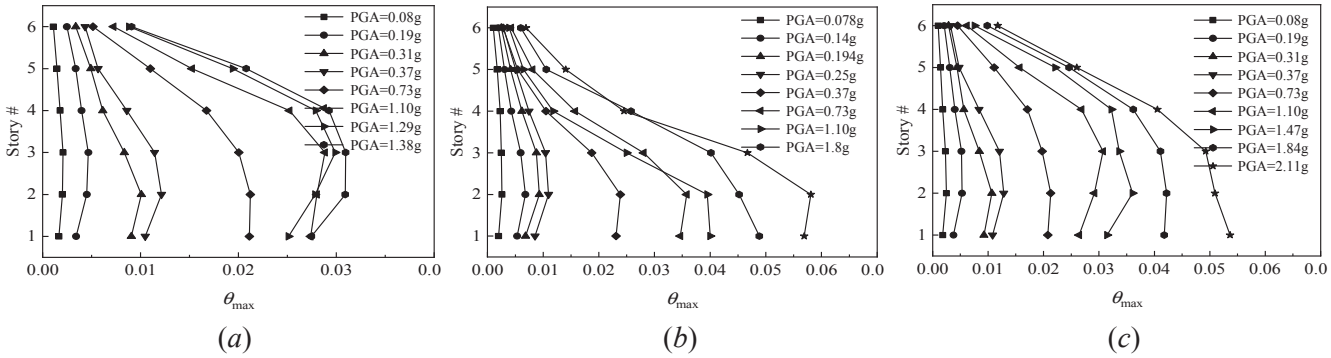


**Fig. 16.** The envelope diagram of $\theta_{max}$ in all stories under #5 earthquake wave for the analyzed frames (a) F0; (b) F1; (c) F2.

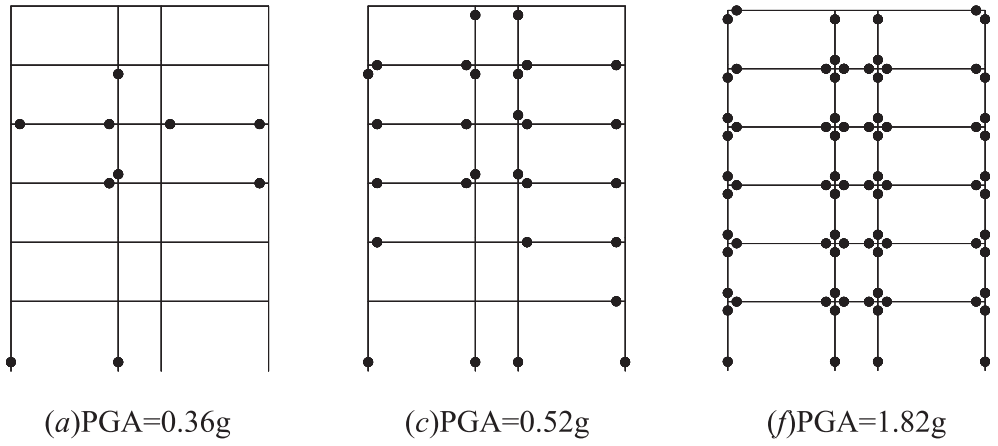


**Fig. 17.** The sequence and distribution of plastic hinges at various PGAs for RC frame.

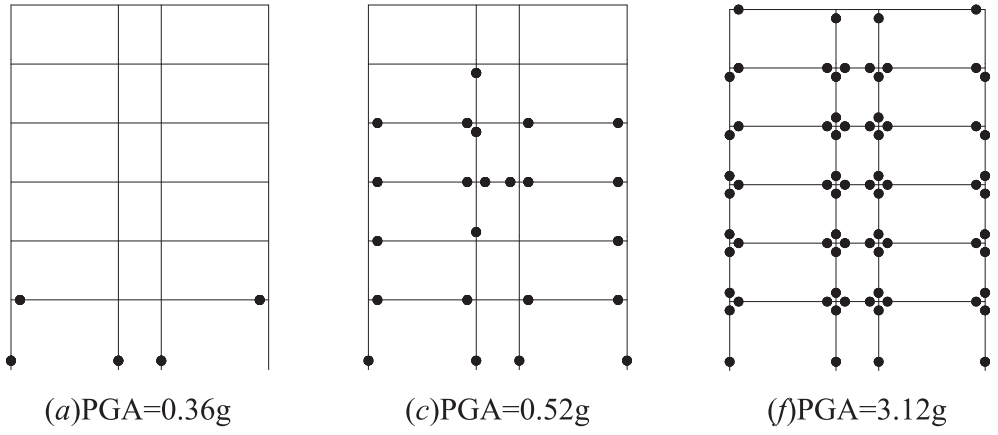


**Fig. 18.** The sequence and distribution of plastic hinges at various PGAs for RECC frame.

critical point for the frames, along with the analogical limit state of $\theta_{max}$ for RC frame in Chinese code for seismic design of buildings (GB50011-2010). Comparing the analytical values of the RC frame with the limit values in GB50011-2010, coincidence is observed in levels I and II, but the analytical $\theta_{max}$ is increasingly larger than the limit state of maximum interstory drift angle at PL III, IV and V. This indicates that the limit state in GB50011-2010 may be excessively conservative.

The comparison among the three frames show that the critical values of $\theta_{max}$ for ECC frame at each performance level is always larger than other frames, closely followed by ECC/RC composite frame, while the critical $\theta_{max}$ of RC frame is far lower. At I and II levels, the critical values of $\theta_{max}$ of ECC frame and ECC/RC frame are 2 and 1.5 as times as the value of RC frame, respectively. Further at III, IV and V levels, the ratio of critical $\theta_{max}$ of ECC frame and ECC/RC frame to RC frame progressively grow to about 2.55 and 1.85 respectively, which indicates that ECC frame and ECC/RC frame have obvious improvement in seismic performance and deformation capacity under moderate and heavy earthquakes.

### 3.5. Cost vs. Performance

Based on the analysis above, it can be concluded that ECC frame and RC frame have the superior and relatively inferior seismic performance respectively, and seismic performance of ECC/RC composite frame falls in between. However, the construction cost of ECC is much higher than normal concrete. In P.R. China, the cost of concrete is inexpensive, and the cost is around 350 RMB/$m^3$ ~ 450RMB/$m^3$ for normal concrete with grade of 35 MPa. While a commonly used PVA fiber in ECC is

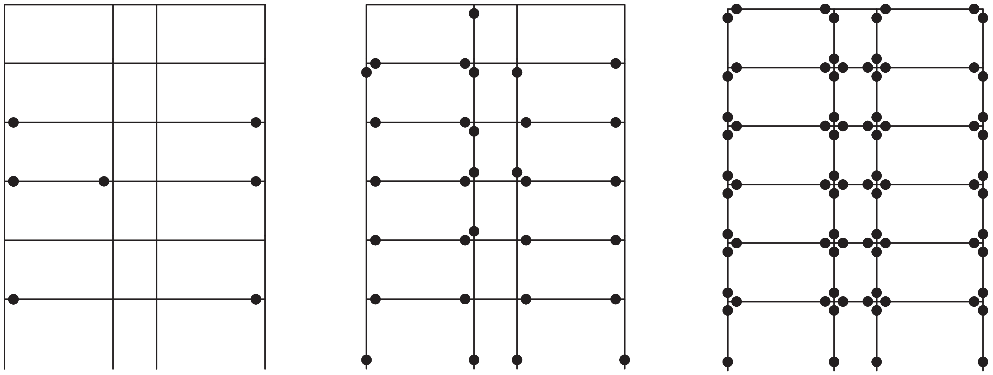


**Fig. 19.** The sequence and distribution of plastic hinges at various PGAs for RECC/RC composite frame.

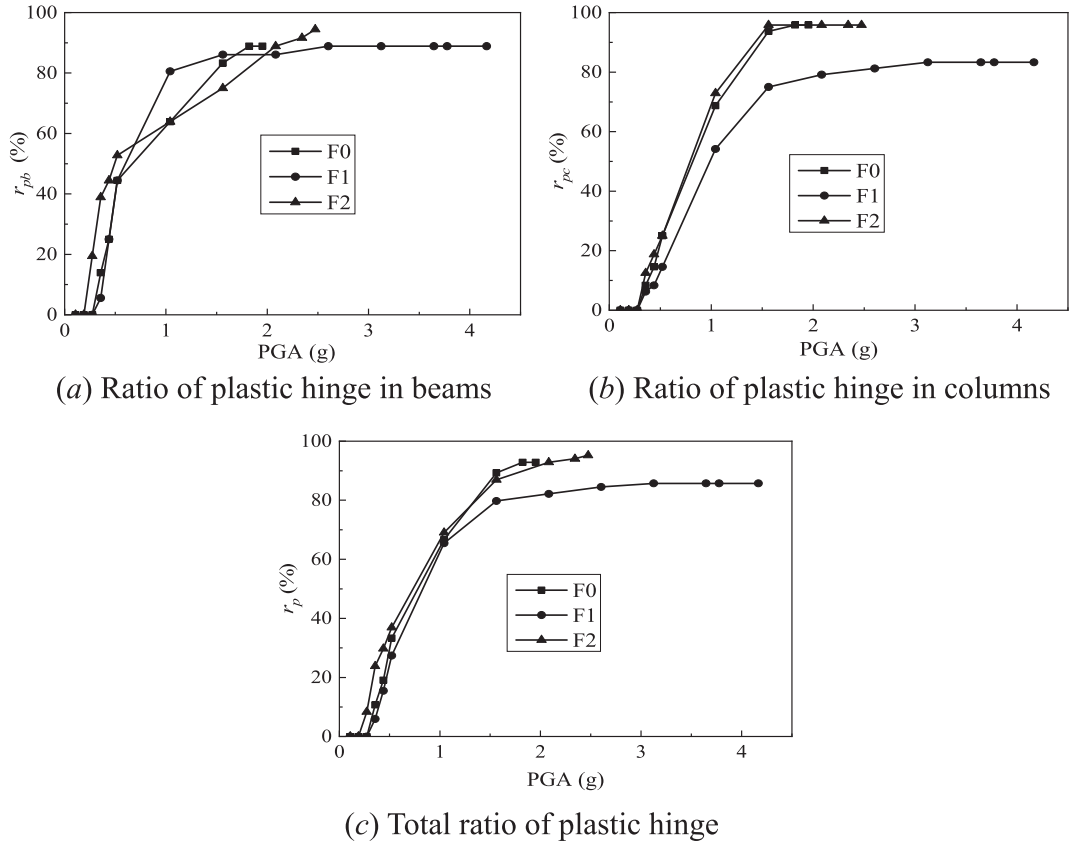


**Fig. 20.** Ratio of plastic hinge vs. PGA.

around 150RMB/kg ~ 180RMB/kg, taking the ECC mixes in reference [39] as an example, the cost of ECC is roughly round 4000 ~ 5200RMB/m$^3$. Assuming that the cost of C35 concrete is 400RMB/m3, while ECC applied in the assumed frames costs 4600RMB/m3, the cost of ECC is about 11.5 times higher than normal concrete in the same volume. Assuming that the construction cost of RC frame is normalized to 1, Table 5 lists the relative construction cost of ECC frame and ECC/RC composite frame normalized by the cost of RC frame. By applying the maximum drift angle $\theta_{max}$ at the PL V as the measurement, Table 5 also lists the relative values of $\theta_{max}$ at PL V normalized by the $\theta_{max}$ of RC frame. It should be noted that the quantitative results in Table 5 can be only limited to the assumed frames, since performance of the RC frame could be improved by optimizing the designing, and consequently reduces the differences between the performances and costs of the different frames. It can be seen from the table that the seismic performance of ECC frame is as 2.6 times as RC frame, however, the construction cost of ECC frame is 10.5 times higher than the RC frame. Although the application of ECC can improve the durability and decrease the post-seismic repairing costs, which makes the cost lower than the value in table in the view of whole life cycle costs, it still hard to persuade the developers to use ECC widely. Comparing to the ECC frame, the seismic performance of ECC/RC composite frame is slightly lower, but is still as 1.9 times as RC frame and the construction cost only increases to 2.4 times of RC frame's. Therefore, only using ECC in particular region, such as joint and plastic hinge areas, can not only improve the seismic performance and deformation capacity of structures but also save material cost, which is a rational way to take full advantage of ECC material. For further saving material cost, ECC can be only applied in the joint area of the story whose plastic deformation is relatively higher than the other stories

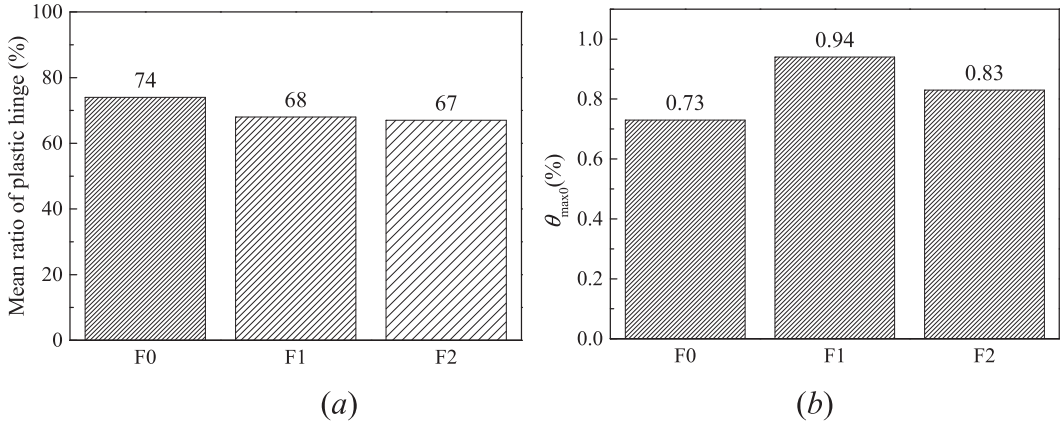


**Fig. 21.** Bar charts of the (a) mean ratio of plastic hinge and (b) $\theta_{max0}$.

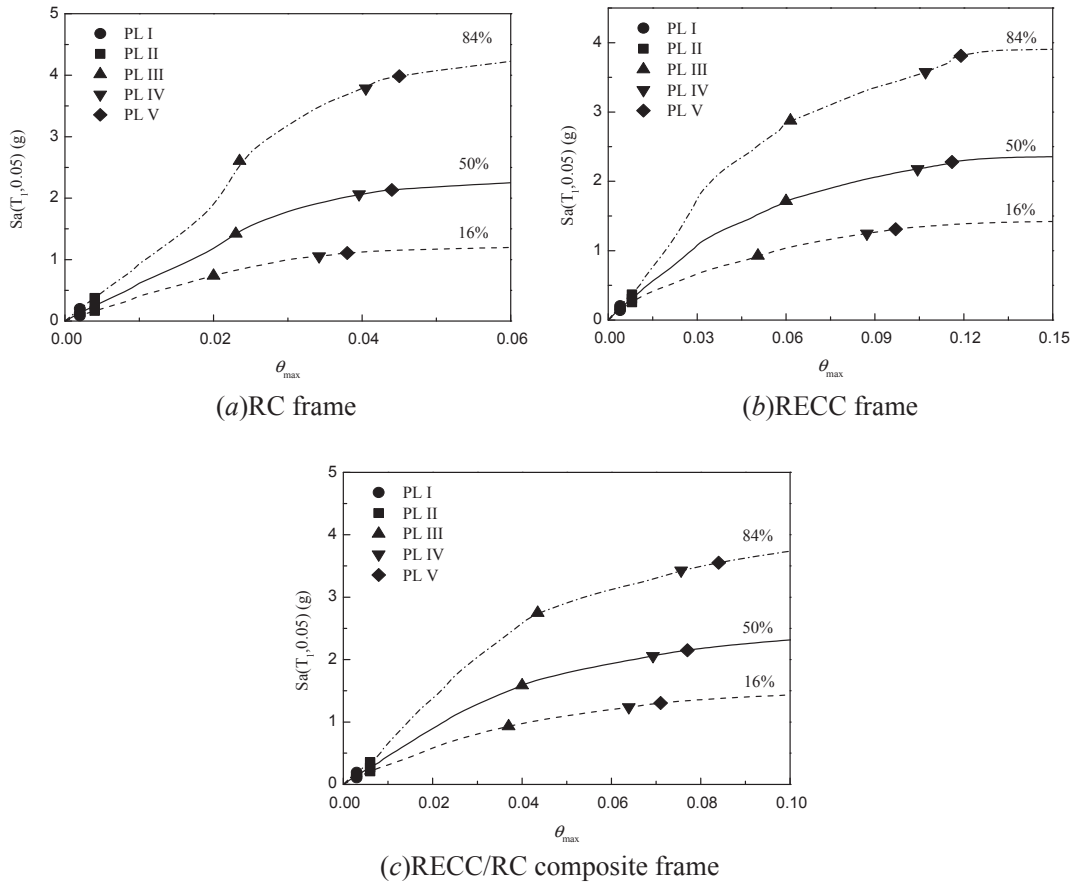


**Fig. 22.** Determination of the PL critical points on different quantile IDA curves.

**Table 4**
Critical values of $\theta_{max}$ at the limit states of performance levels.

| Performance level | Critical values of $\theta_{max}$ /% | | | |
|---|---|---|---|---|
| | Analytical results | | | Limit state in GB50011-2010 (for RC frame) |
| | F0 | F1 | F2 | |
| I | 0.2 | 0.4 | 0.3 | 0.18 |
| II | 0.4 | 0.8 | 0.6 | 0.40 |
| III | 2.0 | 5.1 | 3.7 | 0.83 |
| IV | 3.4 | 8.7 | 6.4 | 1.67 |
| V | 3.8 | 9.7 | 7.1 | 2.00 |

**Table 5**
Construction cost and seismic performance of analyzed frames.

| | F0 | F1 | F2 |
|---|---|---|---|
| Construction cost | 1.0 | 11.5 | 2.4 |
| Seismic performance | 1.0 | 2.6 | 1.9 |

based on the analysis results.

## 4. Conclusion

A series of IDAs have been conducted, aimed at evaluating and comparing the seismic performances of a sample RC frame, a RECC

frame and a RECC/RC composite frame on the basis of Performance-based Seismic Design (PBSD) concept. The cyclic constitutive model was implemented in OpenSEES for simulating the non-linear behavior of ECC material especially considering the strain hardening behavior in tension. The seismic performance of a frame was differentiated to five levels according to the damage intensity and the deformation limit states at the five performance levels were defined in this study. Based on the modeling results and comparisons, the following conclusions can be drawn:

(1) The slope of the IDA curve of RC frame decreased rapidly after a certain value of $\theta_{max}$ is reached; whereas the slopes of the IDA curves of RECC and RECC/RC composite frames decrease gradually, and therefore, their IDA curves grow higher than the curve of RC frame, indicating that RECC frame and RECC/RC frame can undergo more intensive earthquake than normal RC frame.
(2) The analyses and comparison on the $\theta_{max}$ of the assumed frames shows that the $\theta_{max}$ usually located in the second or third story and below, and RECC frame shows the highest interstory drift capacity, followed by ECC/RC composite frame, both of which performed improved deformation capacity compared with normal RC frame.
(3) Comparing the ratio and distribution of plastic hinges, RC frame has the largest mean ratio of plastic hinges at the PL V point, 74%; while the mean ratios for ECC frame and ECC/RC composite frame are 68% and 67%, respectively, both lower than the ratio of RC frame, indicating that more members may be damaged under moderate or strong earthquakes for RC frames, while fewer members may be damaged in ECC frame or ECC/RC composite frame attributed to the larger rotation capacity of the plastic hinges.
(4) Comparative studies on the deformation limit states at five levels of seismic performance for these three different types of frames validated that RECC frames have superior deformation capacity comparing to traditional RC frames under high intensity earthquake, and the seismic performance of RECC/RC composite frame falls in between.
(5) Cost analysis of the assumed frames indicates that the construction cost of ECC is much higher than normal concrete, which leads to excessive cost in construction for frames that entirely constructed with ECC. By discussing the feasibility and practicability of applying ECC in structures for improving the seismic performance, it is indicated that only using ECC in particular region, such as joint and plastic hinge areas, can not only improve the seismic performance and deformation capacity of structures but also save material cost, which is a rational way to take full advantage of ECC material.

## CRediT authorship contribution statement

**Chang Wu:** Conceptualization, Methodology, Software, Formal analysis, Data curation, Writing - original draft, Writing - review & editing. **Zuanfeng Pan:** Conceptualization, Resources, Validation, Funding acquisition. **Chenhua Jin:** Visualization, Investigation. **Shaoping Meng:** Supervision, Project administration.

## Declaration of Competing Interest

The authors declare that they have no known competing financial interests or personal relationships that could have appeared to influence the work reported in this paper.

## Acknowledgement

The authors acknowledge the funding supports of National Natural Science Foundation of China (Grant No. 51411140246 and 51778462).

## References

[1] Li VC, Leung CK. Steady-state and multiple cracking of short random fiber composites. J. Eng. Mech. 1992;118:2246–64.
[2] Li VC, Stang H, Krenchel H. Micromechanics of crack bridging in fiber reinforced concrete. Mater. Struct. 1993;26:486–94.
[3] Li VC. Engineered Cementitious Composites—Tailored composites through micromechanical modeling. In: Banthia, N., Bentur, A., Mufri, A. (Eds.) Fiber-Reinforced Concrete: Present and the Future, Canadian Society for Civil Engineering, 1998, Montreal, Canada, pp. 64-97.
[4] Li VC. Engineered Cementitious Composite (ECC) — Material, structure and durability performance, 2007, CRC Press, Boca Raton, FL, USA.
[5] Yang EH, Wang S, Yang Y, Li VC. Fiber-bridging constitutive law of engineered cementitious composites. J. Adv. Concr. Technol. 2008;6:181–93.
[6] Zhang J, Leung CK, Gao Y. Simulation of crack propagation of fiber reinforced cementitious composite under direct tension. Eng. Fract. Mech. 2011;78:2439–54.
[7] Maruta M, Kanda T, Nagai S, Yamanoto Y. New high-rise RC structure using precast ECC coupling beam. Concrete J. Japan Concrete Institute 2005;43:18–26.
[8] Parra-Montesinos G, Wight JK. Seismic response of exterior RC column-to-steel beam connections. J. Struct. Eng. ASCE 2000;126(10):1113–21.
[9] Kesner K, Billington S. Investigation of infill panels made from engineered cementitious composites for seismic strengthening and retrofit. J. Struct. Eng. 2005;131:1712–20.
[10] Hosseini F, Gencturk B, Aryan H, Cadaval G. Seismic behavior of 3-D ECC beam-column connections subjected to bidirectional bending and torsion. Eng Struct. 2018;172:751–63.
[11] Hou L, Xu R, Chen D, Xu S, Aslani F. Seismic behavior of reinforced engineered cementitious composite members and reinforced concrete/engineered cementitious composite members: a review. Structural Concrete 2019:1–21. https://doi.org/10.1002/suco.201800269.
[12] Lequesne RD, Parra-Montesinos GJ, Wight JK. Seismic behavior and detailing of high-performance fiber-reinforced concrete coupling beams and coupled wall systems. J. Struct. Eng. 2012;139(8):1362–70.
[13] Qudah S, Maalej M. Application of engineered cementitious composites (ECC) in interior beam–column connections for enhanced seismic resistance. Eng. Struct. 2014;69:235–45.
[14] Saghafi MH, Shariatmadar H. Enhancement of seismic performance of beam-column joint connections using high performance fiber reinforced cementitious composites. Constr Build Mater. 2018;180:665–80.
[15] Wu C, Pan Z, Su RKL, Leung CKY, Meng S. Seismic behavior of steel reinforced ECC columns under constant axial loading and reversed cyclic lateral loading. Mater Struct. 2017;50(1):78-1-15.
[16] Xu L, Pan J, Chen J. Mechanical behavior of ECC and ECC/RC composite columns under reversed cyclic loading. J Mater Civ Eng. 2017;29(9):04017097.
[17] Yuan F, Pan J, Xu Z, Leung CKY. A comparison of engineered cementitious composites versus normal concrete in beam-column joints under reversed cyclic loading. Mater Struct. 2013;46(1–2):145–59.
[18] Yuan F, Pan J, Dong L, Leung CKY. Mechanical behaviors of steel reinforced ECC or ECC/concrete composite beams under reversed cyclic loading. J. Mater. Civ. Eng. 2013;26(8). 04014047-1-8.
[19] Gencturk B, Elnashai AS, Lepech MD, Billington S. Behavior of concrete and ECC structures under simulated earthquake motion. J. Struct. Eng. 2012;139(3):389–99.
[20] Gencturk B, Elnashai AS. Numerical modeling and analysis of ECC structures. Mater. Struct. 2013;46(4):663–82.
[21] Gencturk B, Kaymaz I, Hosseini F. Derivation of seismic design parameters for ECC and multi-material special moment-resisting frames. J. Earthquake Eng. 2016;20(7):1054–76.
[22] Yuan F, Pan J, Leung CKY. Elastoplastic time history analysis of reinforced engineered cementitious composite or engineered cementitious composite-concrete composite frame under earthquake action. Adv. Struct. Eng. 2017;20(4):491–503.
[23] Xu L, Pan J, Leung CKY, Yin W. Shaking table tests on precast reinforced concrete and engineered cementitious composite/reinforced concrete composite frames. Adv. Struct. Eng. 2018;21(6):824–37.
[24] Liang X, Lu T. Seismic evaluation of engineered cementitious composites beam–column–slab subassemblies with various column-to-beam flexural strength ratios. Struct. Concrete 2018;19(3):735–46.
[25] Yu J, Ye J, Zhao B, Xu S, Wang B, Yu K. Dynamic response of concrete frames including plain ductile cementitious composites. J. Struct. Eng. ASCE. 2019;145(6):04019042.
[26] Bertero VV. Strength and deformation capacities of buildings under extreme environments. Structral Engineering and Structural Mechanics, 1977, Prentice Hall, New Jersey, USA.
[27] Vamvatsikos D, Cornell CA. Incremental dynamic analysis. Earthquake Eng. Struct. Dyn. 2002;31(3):491–514.
[28] Vamvatsikos D, Cornell CA. Applied incremental dynamic analysis. Earthquake Spectra 2004;20(2):523–53.
[29] Vamvatsikos D, Fragiadakis M. Incremental dynamic analysis for estimating seismic performance sensitivity and uncertainty. Earthquake Eng. Struct. Dyn. 2010;39(2):141–63.
[30] Vamvatsikos D, Cornell CA. Direct estimation of seismic demand and capacity of multi-degree-of-freedom systems through incremental dynamic analysis of single degree of freedom approximation. J. Struct. Eng. 2005;131(4):589–99.
[31] Vamvatsikos D, Cornell CA. Direct estimation of the seismic demand and capacity of oscillators with multi-linear static pushovers through IDA. Earthquake Eng. Struct. Dyn. 2006;35(9):1097–117.

[32] FEMA-356. Prestandard and commentary for the seismic rehabilitation of buildings, Federal Emergency Management Agency, 2000, Washington DC, USA.
[33] National standard of P. R. China. Code for design of concrete structures (GB50010-2010), Building Industry Press, 2010, Beijing, China.
[34] Wu C, Pan Z, Meng S. Cyclic constitutive model for strain-hardening cementitious composites. Mag. Concr. Res. 2016;68(22):1133–42.
[35] Wu C, Pan Z, Mo YL, Li M, Meng S. Modeling of shear-critical reinforced engineered cementitious composites members under reversed cyclic loading. Struct. Concr. 2018;19(6):1689–701.
[36] ATC-63. Quantification of building seismic performance factor (FEMA P695), 2009, Washington DC, USA.
[37] National standard of P. R. China. Code of Seismic Design of Buildings (GB50011-2010). Building Industry Press, 2010, Beijing, China.
[38] National standard of P. R. China. Classification of earthquake damage to buildings and special structures (GB/T 24335-2009), Building Industry Press, 2009, Beijing, China.
[39] Jin C, Wu C, Feng C, Zhang Q, Shangguan Z, Pan Z, et al. Mechanical properties of high-volume fly ash strain hardening cementitious composite (HVFA-SHCC) for structural application. Materials 2019;12(16):2607.